Satellite Image Change Detection using Disjoint Information and Local Dissimilarity Map

Anonymous CVPR submission

Paper ID *****

Abstract

This paper presents a new change detection technique for images taken from the sentinel-2 satellite between 2015 *and* 2018 *in different regions of the world. These images are widely used in recent years for change detection. This technique is based on two dissimilarity measures: the Disjoint Information and the Local Dissimilarity Map. The disjoint information quantifies the dissimilarities between textures and the Local Dissimilarity Map those between structures of images. Firstly, the disjoint information is computed across the blocks of the RGB image channels and the value is multiplied by the center pixel of each block. Secondly, the Local Dissimilarity Maps over the pre-processed channels and the average of the pixel values on the Local Dissimilarity Maps are computed. Finally, an extension of the Gaussian OTSU's threshold are used to detect changes in images. Experimental results on the well-known Onera Satellite Change Detection (OSCD) dataset show the effectiveness of our proposed method compared to the-state-of-the-art deep learning methods.*

Change detection, Disjoint Information, Local Dissimilarity Map, Weibull threshold.

1. Introduction and Related work

Land surface changes are often caused by natural phenomena, human activities or urban growth. In general, land surface changes are divided into two categories: land use and land cover [9]. Land cover describes the physical state of the land surface and land use refers to the way in which the land are exploited by humans [10]. However, change detection has become one of the main problems in the area of image analysis. It consists in detecting the change of two images taken in the same place at different times. This paper focuses on the Onera Satellite Change Detection (OSCD) dataset. The OSCD images are taken between 2015 and 2018 in different regions of the world. They generate time series of multispectral images with resolutions varying between 10m and 60m.

In recent years, many researchers have worked on this dataset and most of them used deep learning methods to detect changes between image pairs. In [1], Bovolo proposed the pixel-based change vector analysis (PCVA) for change detection in very high geometrical resolutions images. It is a unsupervised method that models the changes at different resolution levels defining multitemporal and multilevel parcels. The PCANet is presented by Gao et al. [2] to detect the changes for multitemporal synthetic aperture radar images. This method uses the PCA filters as convolutional filters to exploit the representative neighborhood features from each pixel. In [3], Liu et al. introduced a symmetric convolutional coupling network to detect changes between images. But the method only considers the unchanged pixels. In [4], a deep siamese convolutional neural network (SCNN) using the weighted contrastive loss is trained for optical satellite images. The novelty of this method is that siamese network extracts features directly from the image pairs. In [5], Daudt et al. proposed the two architectures siamese and Early Fusion to detect changes between images, and compare the performances using different number of spectral channels as input. The Early Fusion networks performs better than the siamese networks and the authors obtained good performances by taking four spectral channels as input in the Early Fusion networks. Daudt et al. also present in [6] extensions of the architectures of the previous algorithms. These are three fully convolutional neural network architectures that allow to detect changes on multitemporal pairs of images. The networks are tested in both the RGB and multispectral cases. In [7], Liu et al. proposed a deep depthwise separable convolutional network for change detection. The authors used an improved full convolution network (FCN) called U-Net to separate the changing regions. The best perfomances are given when they consider a network with 23 layers. In [8], Saha et al. proposed Adversarial Auxiliary Classification Generating Networks (ACGAN) to overcome the limited ability of some change detection methods. This unsupervised method is based on deep learning that can handle the large number of bands

in multispectral images. It exploits all spectral bands after grouping them into groups of bands dedicated to the spectrum. From multitemporal images, ACGAN is used to obtain pixelwise deep change hypervector.

The above methods can be distinguished into supervised [4], [5], [6], [7] and unsupervised [1], [3], [8]. Supervised methods need both training and ground truth data. In the case of change detection, these models need a large amount of training data to be able to predict changes on unknown image pairs. In contrast, unsupervised methods do not use training and ground truths data. Usually they rely on some assumptions, such as that unchanged regions should demonstrate a smaller pixelwise difference [3]. To our knowledge, the quoted papers [5], [6], [7] and [8] are the most recent ones using the OSCD dataset. Deep learning methods, although they are effective in detecting changes in satellite images, are generally complex and hard to interpret.

In this paper, we present a new and low complexity change detection method based only on two dissimilarity measures which are the disjoint information [19] and the local dissimilarity map [11]. Disjoint information is a measure from information theory. It is based on joint entropy and gives a scalar which indicates the degree of dissimilarity between two sets. Local dissimilarity map is a measure based on Hausdorff's distance which allows to characterize local differences between two images. The purpose of this method is to generate a binary change map. An extension of the Gaussian OTSU's threshold, based on the Weibull distribution, is used to select the changed pixels. As the unsupervised methods, our proposed approach does not need to use a training and ground truths data. In this work, to detect changes, we converted the RGB images in OSCD dataset into CIE Lab colorspace.

This paper is structured as follows. Section 2 introduces the dissimilarity measures. Section 3 describes the details of the proposed change detection method. Section 4 reports the experimental results. Finally, section 5 concludes the paper.

2. Dissimilarity measures

2.1. Disjoint Information

In this section, we are interested in a measure from information theory: disjoint information [15], [19]. Let two images A and B sampled from image distribution A and B with probability density functions $p(A)$ and $p(B)$, the disjoint information (D) is defined as the joint entropy excluding the mutual information (I):

$$D = H(A,B) - I(A,B), \tag{1}$$

where $H(A) = \sum_{x\in A} p(x)\log p(x)$ is the Shannon entropy of random variable x, and $I(A,B)$ is the mutual information defined by :

$$I(A,B) = H(A) + H(B) - H(A,B) \tag{2}$$

$$= \sum_{x\in A}\sum_{y\in B} p(x,y)\log\frac{p(x,y)}{p(x).p(y)}. \tag{3}$$

As illustrated in Figure 1, the disjoint information corresponds to the joint entropy of A and B, without mutual information. We deduce the following relations:

$$D(A,B) = H(A) + H(B) - 2\times I(A,B) \tag{4}$$

As the mutual information, disjoint information can be computed from the probability densities:

$$D(A,B) = \sum_{x\in A}\sum_{y\in B} p(x,y)\log\frac{p(x).p(y)}{p^2(x,y)} \tag{5}$$

Disjoint information is the Kullback-Leibler divergence of the distribution $p(A).p(B)$ and the square of the joint probability density $p^2(A,B)$. Moreover, it verifies the properties of a distance: minimality, symmetry and triangular inequality.

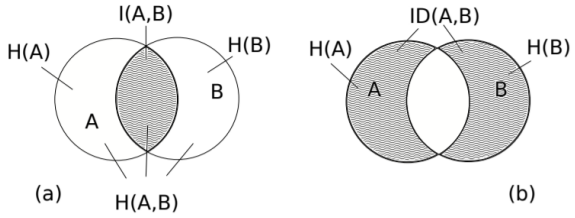

Figure 1. (a) in gray: mutual information $I(A,B)$, (b) in gray: disjoint information. The union of these two sets is the joint entropy $H(A,B)$, the intersection region is the mutual information and disjoint regions are $H(A|B)$ and $H(B|A)$ respectively.

2.2. LDM for grayscale images

The Local Dissimilarity Map (LDM) [11] is an image processing tool allowing to characterize local differences between two images. It is based on the Hausdorff's distance and has produced good results in several research works [13], [14]. Let A and B be two binary images and $p = (x,y)$ the pixel at coordinates (x,y), the LDM is defined from $\mathbb{R}^2\times\mathbb{R}^2$ to $\mathbb{R}^2$ by:

$$\mathrm{LDM}(A,B)(p) = |A(p) - B(p)|\ \max(\mathrm{dt}_A(p), \mathrm{dt}_B(p)), \tag{6}$$

$$= B(p)\ dt_A(p) + A(p)\ dt_B(p), \tag{7}$$

$\mathrm{dt}_A(p)$ is the euclidean distance transform of A, namely the distance between the pixel p and the nearest non-zero pixel of A.

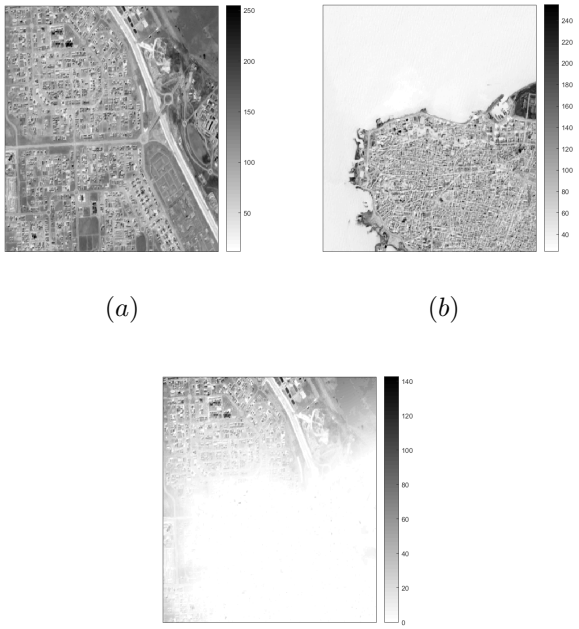

Figure 2. Grayscale image A (a), grayscale image B (b) and the Local Dissimilarity Map of A and B (c).

In [12], Molchanov and Teran have extended the euclidean distance transform to grayscale images. This work has enabled us to adapt the LDM to grayscale images. These are first divided into binary sub-images using thresholds. The grayscale LDM is then computed as the sum of the LDM of each binary image pair. The LDM of two grayscale images A and B is defined from $\mathbb{R}^2$ to $\mathbb{R}^2$ by:

$$\mathrm{RVLDM}(A,B)(p) = \frac{1}{N}\sum_{i=1}^{N}\mathrm{LDM}(A_i,B_i)(p), \qquad (8)$$

where N is the number of thresholds used in the sum, t_i is a threshold, $A_i = \{p \in A : A(p) \geq t_i\}$. Each threshold t_i is chosen according to a regular spacing between $m = \max(\min(A), \min(B))$ and $M = \min(\max(A), \max(B))$. This regular spacing has a step of $s = (M-m)/N$.

Figure 2 shows an example of LDM of two satellite images from OSCD dataset converted in grayscale images. We can see that the areas where the pixel values of the two images have a very large gap are in gray and where they are locally close is white (close to zero).

2.3. LDM for images with C channels

The LDM was only computed on binary and grayscale images. In this work, we propose an extension of the grayscale LDM for images with C channels. In our case, images are converted into the CIE Lab colorspace, which is defined with respect to the CIE XYZ colorspace. The latter provides a color representation that is closer to the human visual system, but the space CIE Lab has the advantage of a distribution of colors more consistent with the perception of color differences by the human visual system. Let A_i be the i^{th} channel of image A in CIE Lab, the $\mathrm{LDM}^{\mathrm{Lab}}$ is defined as:

$$\mathrm{LDM}^{\mathrm{Lab}}(p) = \frac{1}{3}\sum_{i=1}^{3}\mathrm{LDM}(A_i,B_i)(p), \qquad (9)$$

Figure 3 shows four satellite images from two different dates in Brasilia and Montpellier and their Local Dissimilarity Maps. The changes (in dark, Figure 3 (e) and (f)) between satellite images taken at two different times are clearly visible.

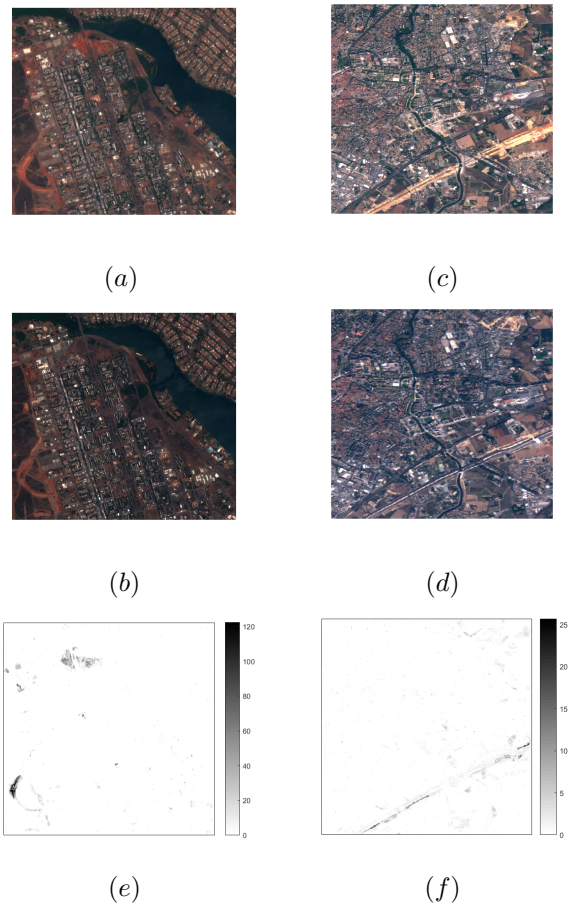

Figure 3. Brasilia on date 1 (a), Brasilia on date 2 (b), Montpellier on date 1 (c), Montpellier on date 2 (d), Local Dissimilarity Map of the two satellite images ((a) and (b)) (e) and the Local Dissimilarity Map of the two satellite images ((c) and (d)) (f) .

3. Proposed Methodology

The purpose of our approach is to generate a binary change map. To achieve this goal, we combined two measures of dissimilarity (LDM and disjoint information) in multispectral satellite images. This paper focuses on color images (RGB, 3 channels). However, the RGB colorspace is converted into the CIE Lab colorspace. Considering channel 1 of image 1 and channel 2 of image 2 in CIE Lab colorspace, the disjoint information which is based on joint entropy, gives a scalar that indicates the degree of dissimilarity between channels. Figure 4 shows the diagram of our change detection method. The full process of our change detection method on color images is detailed below.

3.1. Partitioning of the channels of both images

Firstly, images are divided into 3 channels and each channel is partitioned into lxl overlapping blocks. Blocks overlap with steps of 1 pixel in each channel and the center pixel of each block is the pixel of interest.

3.2. Calculation of disjoint information between blocks

Disjoint information is a criterion that measures the amount of information contained by one variable in comparison to another. As indicated in the previous section, for each pixel location, there are two blocks which are obtained from channel A_i of the first image and channel B_i of the second image. Hence, disjoint information is computed on blocks for each pixel location. Therefore, in this work, it is considered as spatial neighborhood disjoint information. The main advantage of this measure is that it does not require any prior relationship between images. It is based on the statistical relationship of variables or images joint entropy [15].

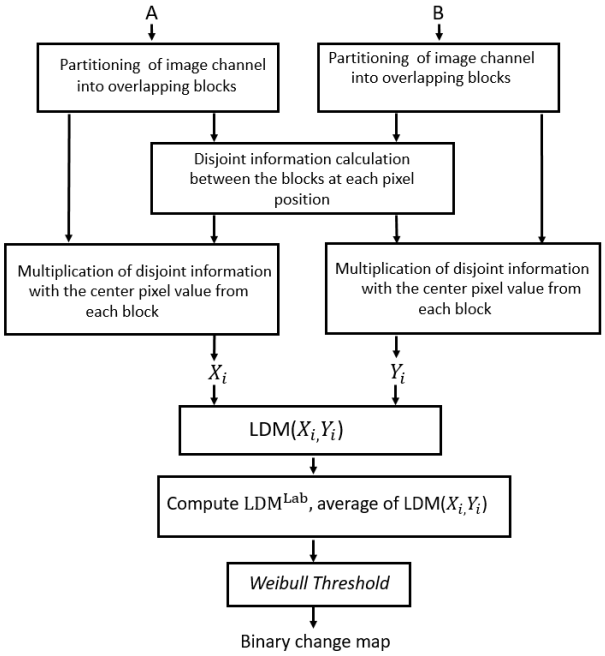

Figure 4. Block diagram of the proposed technique.

Let α and β be two sliding blocks from the channels A_i and B_i. Disjoint information on blocks is defined as follows (eq.(4)):

$$D_{\alpha,\beta}(x,y) = H(\alpha) + H(\beta) - 2 \times I(\alpha,\beta) \quad (10)$$
$$= 2 \times H(\alpha,\beta) - H(\alpha) - H(\beta) \quad (11)$$

where $H(\alpha)$ and $H(\beta)$ are the entropies of the blocks of A_i and B_i respectively, $I(\alpha,\beta)$ is the mutual information of the blocks and $H(\alpha,\beta)$ is the joint entropy between blocks.

3.3. Merge LDMs between different channels.

As mentioned above, disjoint information is calculated on the blocks of the channels of both color images. After that, spatial neighborhood disjoint information of each pixel location is multiplied by the value of the center pixel of the blocks. This will allow to transform the textures containing in the channels to structures in order that the LDM be adapted. As in [11], the LDM works better on images containing only structures. In [20], Gupta et al. proposed a similar approach but with mutual information.

The pixel value for each pixel location for both A_i and B_i channels are computed as follows:

$$X_i(x,y) = D_{\alpha,\beta}(x,y) \times \alpha(x,y) \quad (12)$$
$$Y_i(x,y) = D_{\alpha,\beta}(x,y) \times \beta(x,y) \quad (13)$$

where (x,y) is the pixel location with $x = \{1,....,m\}$ and $y = \{1,....,n\}$; m and n are the channel sizes.
The Local Dissimilarity Map between channels then becomes eq.(9):

$$\mathrm{LDM}^{\mathrm{Lab}}(x,y) = \frac{1}{3}\sum_{i=1} \mathrm{LDM}(X_i,Y_i)(x,y), \quad (14)$$

where $\mathrm{LDM}(X_i,Y_i)$ is the LDM between the i^{th} preprocessed channels of the image A and the image B.

3.4. Thresholding to generate the change detection map

3.4.1 OTSU threshold selection method

Threshold selection is a method used in unsupervised approaches to generate binary change maps. OTSU threshold is the popular method which maximizes variances between changed and unchanged pixels to get an optimal threshold [16]. The OTSU algorithm assumes the image to be binarized contains only two classes: the foreground pixels

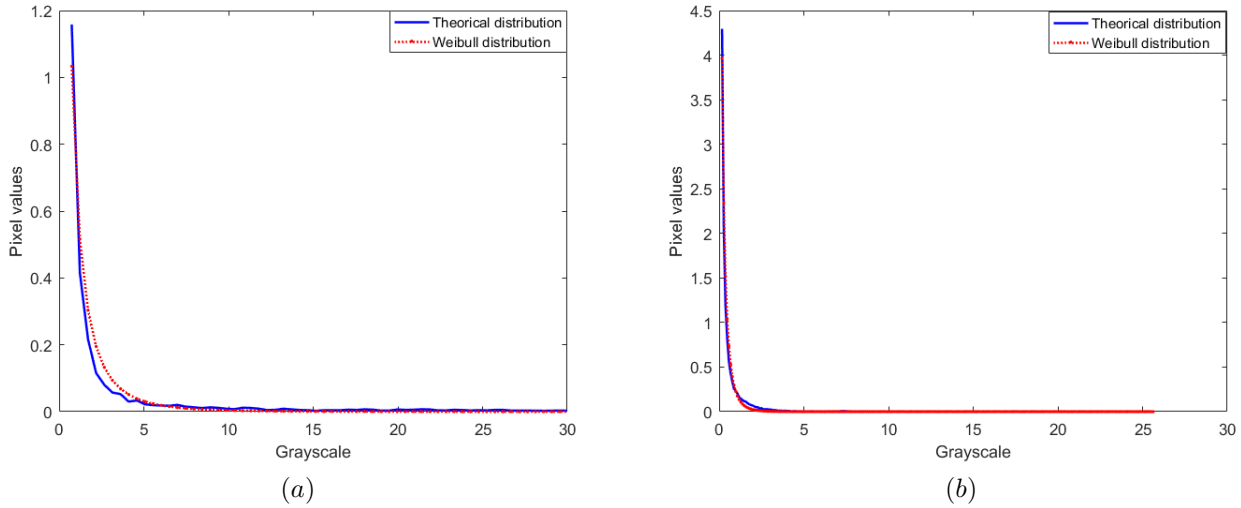

Figure 5. The histograms of the Local Dissimilarity Maps fitted by a two-parameter Weibull distribution. The Figures (a) and (b) are respectively for the Local Dissimilarity Map of satellite images in Figure 3 (e) and Figure 3 (f).

and the background pixels. The iterative algorithm calculates the optimal threshold separating these two classes in order to minimize the intraclass variance (V) and the interclass variance $(V1)$.

The optimal threshold V can be determined by maximizing the following criteria with respect to $V1$:

$$\eta = \omega_0\omega_1(\mu_0 - \mu_1), \tag{15}$$

where ω_0 and ω_1 are the probabilities of the two classes separated by a threshold t, μ_0 and μ_1 are the averages of the two classes.

Finally, pixel value can be classified as change or no change with respect to the following formula:

$$t(k) = \begin{cases} change & \text{if } d(k) > V \\ no\ change & \text{otherwise.} \end{cases} \tag{16}$$

In our case, $d(k)$ is the pixel values of $\mathrm{LDM}^{\mathrm{Lab}}$.
This thresholding method is based on a Gaussian distribution.

3.4.2 Weibull threshold method

The method presented in the previous section is Gaussian Otsu's method. It is an extension of Otsu thresholding technique based on intra-class variance from the foreground and background regions.

Since the pixel values of a LDM follow a Weibull distribution [18], instead of using the Gaussian distribution for the threshold calculation, we used the Weibull distribution. The Figure 5 shows the histograms of the Local Dissimilarity Maps in Figure 3 (e) and Figure 3 (f), fitted by Weibull distributions. The shape and scale parameters of Weibull extracted from each LDM are used to represent histograms and mainly the probability of each pixel.

Algorithm 1 Weibull threshold method

1. Input LDM
2. Compute histogram with the Weibull parameters extracted from LDM
3. Compute probabilities of each intensity level
4. Browse all possible thresholds t = 1,...,N
   - Update ω_i, μ_i
   - Compute η_i
5. Threshold corresponds to the maximum η_i

N is the maximum intensity.

The difference between the two thresholds is the way the histogram is computed.

4. Experimental results

4.1. User dataset

To evaluate the proposed change method we used the Onera Satellite Change Detection (OSCD) dataset openly available. It is a dataset that focuses only on urban growth and changes ignoring natural changes [5]. The Figures 6 and 7 show examples of satellite image pairs and the associated change maps.

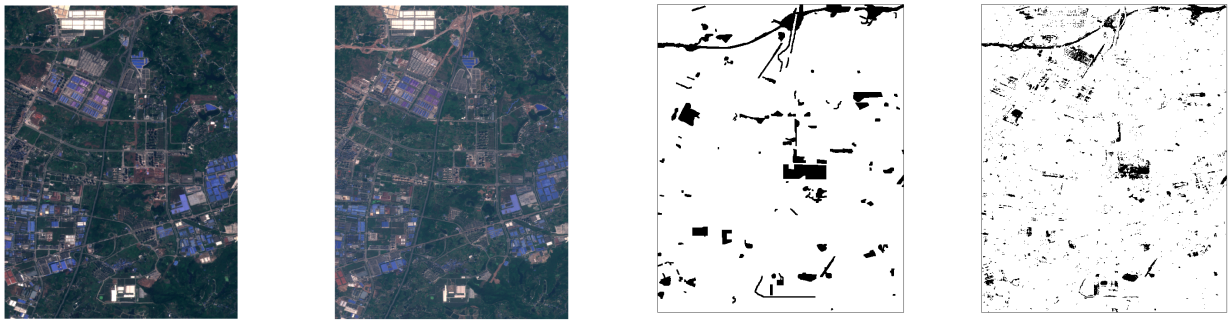

(a) (b) (c) (d)

Figure 6. Results of the change detection on the Chongqing test images. Chongqing 2017-04-14 (a), Chongqing 2017-04-02 (b), ground truth (c), proposed method (d).

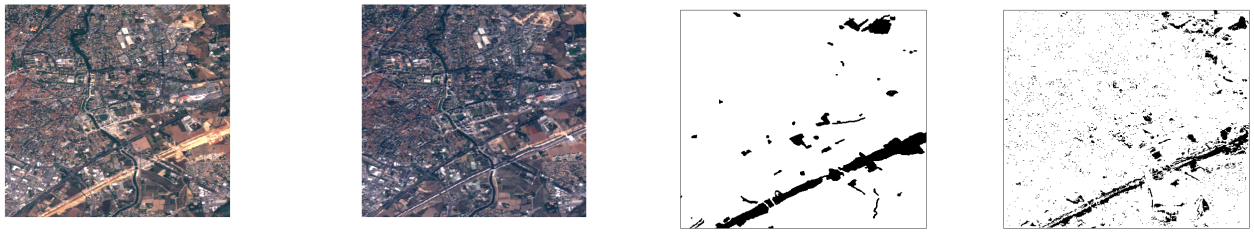

(e) (f) (g) (h)

Figure 7. Results of the change detection on the Montpellier test image. Montpellier 2015-08-12 (e), Montpellier 2017-10-30 (f), ground truth (g), proposed method (h).

Table 1. Change detection results for OSCD dataset.

Algorithm	Method	Sensitivity (%)	Specificity(%)	Overall accuracy (%)
Unsupervised	Ours	54.8	84.9	90.8
	Saha [8]	64.6	78.3	77.6
	PCVA [8]	47.0	75.6	74.1
Supervised	Liu [7] 13 layers	48.1	91.3	89.1
	Liu [7] 18 layers	68.9	93.3	92.0
	Liu [7] 28 layers	73.8	92.8	91.7
	CNN [7]	50.9	91.7	89.5
	SCNN [7]	48.2	94.8	92.5
	Siam. [5]	74.1	75.23	75.2
	EF [5]	80.3	90.1	89.6

The dataset contains 24 pairs (14 pairs for training and 10 pairs for testing) of multispectral images (13-band) taken from the Sentinel-2 satellite between 2015 and 2018 in different regions of the world. Images vary in spatial resolution between 10m, 20m and 60m. Since our approach is unsupervised, we do not need to use the training dataset. Performances are only evaluated on the 10 test image pairs as in [8] that provides performance indices considering all the pixels from the 10 test images.

In this paper, we worked only on RGB images and they are converted to CIE Lab colorspace before applying our change detection method.

4.2. Choice of block size

The size blocks that were tested in this work are from 3 to 21 with steps of 2. Figure 8 shows the relationship between block sizes and the (%) of correct changes for image pairs from Montpellier and Chongqing. We can see that the

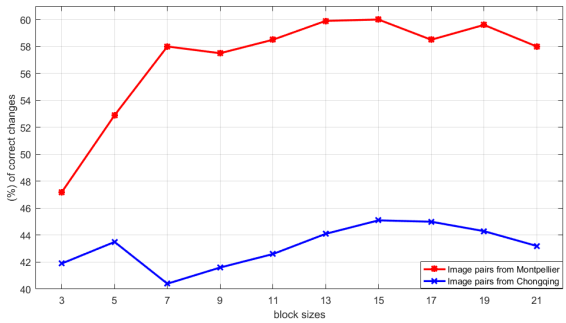

Figure 8. Relationship between block sizes and (%) of correct changes for image pairs from Montpellier and Chongqing.

choice of block size is robust from 9, but the block with size 15 gave the best score for correct changes. Therefore, we considered this block size in the rest of our work to show the effectiveness of our proposed method.

4.3. State of art methods for comparison

In this section, we compare the proposed method with some supervised [5], [7] and unsupervised [8] methods. We provide comparisons in terms of sensitivity (accuracy of correct changes), specificity (accuracy of unchanged pixels) and overall accuracy [8].

4.4. Results for the OSCD dataset

For the ten images of OSCD, the proposed method gives a sensitivity of 54.8%, a specificity of 84.9% and overall accuracy of 90.8%. Results of our approach and the state-of-the-art methods can be seen in table 1. Saha's method [8] outperforms ours in terms of sensitivity. This is due to the fact that Saha [8] used a data set targeted for image classification to train the ACGANs. The authors have trained 4 ACGANs. Thus, it is a method that requires training network before using the test images. In contrast, we obtained best performances in terms of specificity and overall accuracy compared to the unsupervised methods. The proposed method is comparable in performances with the supervised methods such as CNN, SCNN and Liu [7] with 13 layers in terms of sensitivity and overall accuracy. We outperform the supervised siamese method in terms of specificity and overall accuracy. However, the supervised methods such as the early fusion (EF) [5] and Liu [7] (with 18 and 28 layers) performs better than our method in terms of sensitivity, specificity and potentially the overall accuracy. The main benefit of these approaches is that they are supervised and they use multitemporal labelled data to learn to extract change information.

Although supervised methods give good results, they are sometimes complex, hard to interpret and they also need a large amount of data for the network training. The unsupervised proposed method in [8] also needs to train the ACGANS network. We propose a low complexity technique that does not require model learning and the results show the effectiveness of our method compared to those in the state-of-the-art.

5. Conclusion and future work

This paper presented a new and low complexity change detection method based on Disjoint Information and the Local Dissimilarity Map. An extension of the Gaussian OTSU's method is used to establish the binary change maps. The proposed method is applied on the Onera Satellite Change Detection method. Compared to supervised and unsupervised methods in the state-of-the-art, which used the same dataset, our method has good performances in terms of specificity and overall accuracy and also sensitivity over certain methods.

Results are obtained on colour images converted to the CIE Lab colorspace (3 channels). The dataset OSCD contains multispectral images (13 channels) and the results of some state-of-the-art [7], [8] methods are obtained on the 13 channels. We will then apply our change detection technique on more channels in the future work. However, some channels contain contrasts which are sensitive for the LDM. A Local Contrast Normalization method [17] will be proposed to overcome this problem.

References

[1] Francesca Bovolo. A Multilevel Parcel-Based Approach to Change Detection in Very High Resolution Multitemporal Images. In IEEE Geoscience and Remote Sensing Letters, vol. 6, no. 1, pp. 33-37, Jan. 2009, doi: 10.1109/LGRS.2008.2007429.

[2] Feng Gao, Junyu Dong, Bo Li, and Qizhi Xu. Automatic Change Detection in Synthetic Aperture Radar Images Based on PCANet. In IEEE Geoscience and Remote Sensing Letters, vol. 13, no. 12, pp. 1792-1796, Dec. 2016, doi: 10.1109/LGRS.2016.2611001.

[3] Jia Liu, Maoguo Gong, Kai Qin, and Puzhao Zhang. A Deep Convolutional Coupling Network for Change Detection Based on Heterogeneous Optical and Radar Images. In IEEE Transactions on Neural Networks and Learning Systems, vol. 29, no. 3, pp. 545-559, March 2018, doi: 10.1109/TNNLS.2016.2636227.

[4] Yang Zhan, Kun Fu, Menglong Yan, Xian Sun, Hongqi Wang, and Xiaosong Qiu. Change Detection Based on Deep Siamese Convolutional Network for Optical Aerial Images. In IEEE Geoscience and Remote Sensing Letters, vol. 14, no. 10, pp. 1845-1849, Oct. 2017, doi: 10.1109/LGRS.2017.2738149.

[5] Rodrigo Caye Daudt, Bertrand Le Saux, Alexandre Boulch, and Yann Gousseau, 2018, July. Urban Change Detection for Multispectral Earth Observation Using Convolutional Neural Networks. In IEEE International Geoscience and Remote Sensing Symposium (IGARSS) 2018 (pp. 2115-2118). IEEE.

[6] Rodrigo Caye Daudt, Bertrand Le Saux, and Alexandre Boulch. Fully Convolutional Siamese Networks for Change Detection. IEEE International Conference on Image Processing (ICIP), october 2018.

[7] Ruochen Liu, Dawei Jiang, Langlang Zhang, and Zetong Zhang. Deep Depthwise Separable Convolutional Network for Change Detection in Optical Aerial Images. In IEEE Journal of Selected Topics in Applied Earth Observations and Remote Sensing, vol. 13, pp. 1109-1118, 2020, doi: 10.1109/JSTARS.2020.2974276.

[8] Sudipan Saha, Yady Tatiana Solano-Correa, Francesca Bovolo, and Lorenzo Bruzzone. Unsupervised Deep Transfer Learning-Based Change Detection for HR Multispectral Images. In IEEE Geoscience and Remote Sensing Letters, vol. 18, no. 5, pp. 856-860, May 2021, doi: 10.1109/LGRS.2020.2990284.

[9] Michael J. Barnsley, Lasse Moller-Jensen, and Stuart L. Barr. Inferring urban land use by spatial and structural pattern recognition. Remote sensing and urban analysis, pp. 115-144, 2001.

[10] Jwan Al-doski, Shattri B. Mansor and Helmi Zulhaidi Mohd Shafri. Change Detection Process and Techniques. IISTE: E-journals, vol.3, No 10, 2013.

[11] Étienne Baudrier, Frédéric Morain-Nicolier, Gilles Millon, Su Ruan. Binary-image comparison with local-dissimilarity quantification. Journal of the pattern recognition society, Pattern Recognition, vol. 41, pp. 1461 – 1478, 2008.

[12] Ilya. S. Molchanov and Pedro Teran. Distance transforms for real-valued functions. Journal of Mathematical Analysis and Applications, vol. 278, pp. 472–484, 2003.

[13] Frédéric Morain-Nicolier, Jérôme Landré, Su Ruan. Gray Level Local Dissimilarity Map and Global Dissimilarity Index for Quality of Medical Images. In Proceedings of the 7th IFAC Symposium on Modelling and Control in Biomedical Systems Aalborg, Denmark, Volume 42, Issue 12, pp. 281-286, 2009.

[14] Amar Mardani, Amina Kharbach, Mohammed Rahmoun, Benaissa Bellach, M. Elhitmy. Local and Global Measure of Dissimilarity between Two Segmentations. International Journal of Innovative Technology and Exploring Engineering (IJITEE), Volume-4 Issue-6, pp. 2278-3075, 2014.

[15] Zhaohui Sun and Anthony Hoogs. Image Comparison by Compound Disjoint Information with Applications to Perceptual Visual Quality Assessment, Image Registration and Tracking. International Journal of Computer Vision, vol. 88, pp. 461–488, 2010.

[16] Liang Li, Xue Li, Yun Zhang, Lei Wang, and Guowei Ying. Change detection for high-resolution remote sensing imagery using object oriented change vector analysis method. In Proceedings of the 36th International Geoscience and Remote Sensing Symposium, IGARSS '16, pp. 2873–2876, IEEE, Beijing, China, July 2016.

[17] Kevin Jarrett, Koray Kavukcuoglu, Marc'Aurelio Ranzato, and Yann LeCun. What is the best multi-stage architecture for object recognition? 2009 IEEE 12th International Conference on Computer Vision, 2009, pp. 2146-2153, doi: 10.1109/ICCV.2009.5459469.

[18] Moustapha Diaw, Agnès Delahaies, Jérôme Landré, Frédéric Morain-Nicolier, and Florent Retraint. Fast process for classifying structural image pairs using Weibull parameters extracted from undersampled Local Dissimilarity Maps. 2021 29th European Signal Processing Conference (EUSIPCO), To appear.

[19] Thomas M. Cover and Joy A. Thomas. Information theory and statistics.In Elements of Information Theory, New York, NY, USA: Wiley, pp. 279–335, 1991.

[20] Neha Gupta, and Samit Ari. Spatial Neighborhood Mutual Information based Satellite Image Change Detection. 5th International Conference for Convergence in Technology (I2CT) pp. 29-31, India 2019.